

Why planar cracks fragment into echelon cracks

Olivia Ward¹ and Aditya Kumar²

¹George W. Woodruff School of Mechanical Engineering, Georgia Institute of Technology, Atlanta, GA 30332, USA
²School of Civil and Environmental Engineering, Georgia Institute of Technology, Atlanta, GA 30332, USA

Predicting the growth of large cracks in brittle materials remains a central unresolved problem in fracture mechanics, particularly under out-of-plane shear loading, where an initially planar crack may spontaneously fragment into multiple cracks, forming an echelon crack pattern. In this Letter, through comparison with a classical experiment, we show that a strength-constrained energy-minimization model explains echelon crack formation and provides a unified description of when and where cracks grow in both hard and soft brittle materials. We identify two key non-dimensional parameters governing crack orientation and morphology, and demonstrate that the ratio of shear to tensile strength controls whether crack paths follow energy-based or stress-based empirical criteria, thereby reconciling these approaches within a single theoretical framework.

The analysis of the growth of pre-existing large cracks in brittle materials such as glass or rubber is commonly separated into two questions: (i) when a crack grows, and (ii) where it grows. The first question was resolved more than a century ago by Griffith [1]; along a known path, a crack grows when

$$-\frac{\partial \mathcal{W}}{\partial \Gamma} \leq G_c, \quad (1)$$

where G_c is the fracture toughness, \mathcal{W} is the strain energy, and Γ denotes the crack length (or area); however, experimental validation, especially in soft elastic brittle materials, was not completed until much later. By contrast, the second question, concerning the crack path and morphology, is considerably more challenging. When a planar crack is subjected to loading that is not purely tensile (mode I), it may deviate from its original plane through either abrupt kinking or gradual curving. Under predominantly anti-plane shear (mode III) loading, the parent crack front often undergoes a sudden fragmentation into multiple, initially disconnected daughter cracks [2–6]. Owing to their characteristic stepped geometry, these fracture patterns are commonly referred to as *echelon* cracks (Fig. 1).

One of the earliest experimental investigations of echelon crack growth was performed by Knauss [3], who conducted tearing tests on thick, notched plates of Solithane polymer. He observed the emergence of echelon cracks inclined at approximately 45° to the original crack axis; see Fig. 1(a–b). Subsequent studies have reported echelon crack formation in a broad range of brittle materials, including glass, rocks, polymers, and hydrogels [4, 7–9]. Their occurrence is known to depend on a combination of geometric and loading conditions, as well as intrinsic material properties. Experiments on hydrogels further indicate that echelon crack formation depends on the intrinsic material length scales at the crack tip [4].

Existing fracture theories have failed to explain the formation and growth of echelon cracks. Two fundamental questions arise: (i) why does the crack fail to propagate in a self-similar manner along the axis of the pre-existing

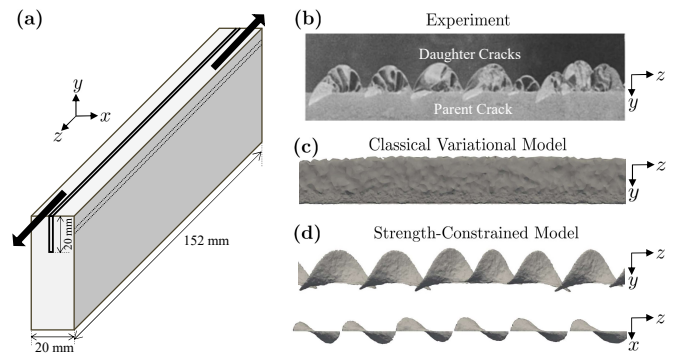


Figure 1. (a) Schematic of the tearing test over a thick plate with the initial parent crack from Knauss [3]. (b) Experimental observation of echelon crack growth. The parent crack fragments into multiple daughter cracks. (c) Crack path predicted by classical variational phase-field model (3). (d) Path predicted by the strength-constrained phase-field model (9). Only the daughter cracks are shown from two views.

crack [10], and (ii) if the crack tends to propagate out of its original plane, why does it do so through fragmentation into multiple cracks rather than via smooth, continuous deviation?

The first question has been examined using the various empirical crack path criteria proposed in the literature since the 1960s [11–15], together with the Griffith criteria (1). Broadly, these criteria, developed primarily for linear elastic, isotropic materials, fall into two classes: (i) energy-based criteria, which postulate crack growth along paths of maximum energy release rate [14], and (ii) local stress-field-based criteria, which postulate that the crack selects a path that locally restores mode I conditions [16]. For many two-dimensional crack growth problems in compressible isotropic materials, these criteria often lead to similar predictions. However, their extensions to three dimensions, nonlinear elastic or anisotropic materials, are highly nontrivial [17]. Proposed 3D extensions in the literature indicate that, for the experimental configuration studied by Knauss (Fig. 1) and other similar mode III tests, energy-based criteria predict continued

planar crack growth [18, 19]. In contrast, stress-based criteria such as the Maximum Tangential Stress (MTS) criterion or the Principle of Local Symmetry (PLS) generally predict that the crack will smoothly curve out of the plane [16]. Similar theoretical models have seen limited development in soft materials.

To explain why an out-of-plane crack fragments into multiple cracks, several empirical hypotheses have been proposed. One suggests that, under mixed-mode I+III loading, sinusoidal or helical perturbations of the crack front become unstable [20, 21]; however, the associated linear instability criteria lack experimental support. Moreover, recent experiments indicate that fragmentation arises from the nucleation of disjointed daughter cracks, rather than from the continuous evolution of an unstable crack front [4, 5, 22]. Another view holds that a smoothly curving crack cannot maintain locally mode I conditions and therefore must fragment, although this has not been simulated, and the underlying rationale for local mode I growth and its general applicability are not understood.

Thus, a fundamental problem in fracture, even in the simplest class of materials, remains unresolved. Addressing this gap requires a theoretical and computational framework that can predict this phenomenon, while also providing a general description of crack nucleation and propagation across arbitrary loading and geometrical configurations, rather than being tailored specifically to the echelon crack problem. Over the past two decades, the development of the variational theory of brittle fracture [23] has raised the prospect of such a unified framework for determining both when and where cracks grow. In this theory, the deformation field $\mathbf{y}(\mathbf{X}, t)$ and the crack set $\Gamma(t)$ are obtained by globally minimizing the total energy, defined as the sum of elastic and fracture contributions:

$$\mathcal{E}(\mathbf{y}, \Gamma) := \int_{\Omega_0 \setminus \Gamma} W(\mathbf{F}) d\mathbf{X} + G_c \mathcal{A}(\Gamma), \quad (2)$$

where $\mathcal{A}(\Gamma)$ stands for the surface measure of the unknown crack and $W(\mathbf{F})$ stands for the hyperelastic energy function of the deformation gradient tensor, \mathbf{F} . This variational formulation provides a mathematically rigorous description of crack growth without recourse to empirical stress-based criteria. Several fundamental mathematical questions have remained open. For instance, even when global minimality in the sharp theory is relaxed to a notion of local stability (metastability), analysis show that crack kinking is incompatible with smooth crack evolution [17, 24, 25].

Nevertheless, this approach has been highly successful in predicting the growth of large pre-existing cracks across a wide range of linear and nonlinear boundary-value problems. For numerical simulation, the sharp crack formulation is commonly regularized using a phase-field approximation [26]. A phase field $z = z(\mathbf{X}, t)$ is

introduced to regularize the crack surface, which takes values in the range $[0, 1]$ over a phase boundary of infinitesimal width ε . Precisely, $z = 1$ identifies regions of the sound material, whereas $z < 1$ identifies regions of the material that have been fractured. The pair of displacement field and phase field minimizes the functional

$$\mathcal{E}^\varepsilon(\mathbf{y}, z) = \int_{\Omega_0} \left[z^2 \mathcal{W}(\mathbf{F}) + \frac{3G_c}{8} \left(\frac{1-z}{\varepsilon} + \varepsilon \nabla z \cdot \nabla z \right) \right] d\mathbf{X}, \quad (3)$$

subject to the irreversibility condition on the phase field. The regularized functional \mathcal{E}^ε in (3) Γ -converges to \mathcal{E} in (2) for $\varepsilon \rightarrow 0$. The success of this formulation for a wide range of problems has fostered the view that the variational framework largely resolves the classical problem of the growth of large cracks in brittle materials initiated by Griffith.

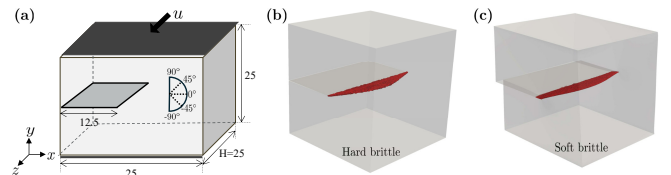


Figure 2. (a) Schematic of a smaller geometry used for comprehensive analysis (all dimensions are in mm; applied displacement in z -direction). (b) Crack path contour obtained from the variational model for a hard brittle material, Graphite, and (c) contour for soft brittle material, PDMS.

However, when we applied the variational phase-field model to simulate Knauss's experiment, echelon crack growth is not reproduced; instead, the model predicts continued planar crack propagation, as shown in Fig. 1(c). Owing to the substantial computational cost associated with the three-dimensional experimental-scale geometry, we adopt a reduced geometry for further analysis (Fig. 2(a)), which enables a more detailed study. The analysis is conducted for two isotropic brittle materials representing hard and soft responses: graphite, modeled as a linear elastic material, and PDMS, modeled as a nearly incompressible nonlinear elastic material. Material parameters for graphite are taken from [27, 28], and those for PDMS from [29, 30], included in Supplemental Material [31]. The results obtained with the reduced geometry for graphite and PDMS are shown in Fig. 2(b–c). In both cases, the model again predicts planar crack growth. The variational phase-field framework has previously been applied to study echelon cracking in hard brittle materials, with similar outcomes reported [18, 32]. In those studies, it was argued that echelon crack growth can be recovered by introducing material disorder—through defects or stochastic fracture toughness—and by modifying the variational formulation via a spectral strain-energy decomposition. In End Matter Appendix A, we show that the use of the energy decomposition is unphysical and not needed for the present

problem. We therefore conclude that the variational formulation, rooted in energy competition, is insufficient to predict echelon crack growth. Thus, contrary to the widespread belief in the literature, it should be considered fundamentally incomplete for predicting large crack growth under tensile/shear regimes.

Classical variational phase-field models lack a critical capability: the ability to describe crack nucleation. This limitation arises from the absence of a strength criterion. While strength is often deemed unnecessary for analyzing the growth of large pre-existing cracks in the literature, recent experiments have cast echelon crack formation as a nucleation problem rather than a continuous evolution of the parent crack front [5]. Motivated by these experiments, we investigate the tearing problem using a strength-constrained phase-field formulation. Such a formulation has been developed in recent years [28, 33] and extensively validated across a wide range of nucleation and propagation scenarios in both soft and hard materials [30, 34–38]. Notably, the formulation has been validated recently for a broad range of mixed-mode fracture problems [39].

In this formulation, the material strength is represented as a surface in three-dimensional stress space, known as the strength surface. This surface defines the set of critical stress states \mathbf{S} at which the material fractures under monotonically increasing, spatially uniform, but otherwise arbitrary loading. Such a set is represented as

$$\mathcal{F}(\mathbf{S}) = 0. \quad (4)$$

For isotropic materials, a simple choice is the two-parameter Drucker–Prager (DP) strength surface, which has been shown to capture the fracture strength of many nominally brittle materials.

The strength surface violation acts as a necessary but not sufficient condition for crack evolution [37]. It acts as a constraint on the variational formulation. Mathematically, we can state it as the following [40]: the deformation field $\mathbf{y}(\mathbf{X}, t)$ and the crack set $\Gamma(t)$ minimize the functional (2) among all

$$\Gamma \subset \mathcal{V}_{\mathcal{F}}(t), \quad (5)$$

where $\mathcal{V}_{\mathcal{F}}(t) = \{\mathbf{X} : \mathcal{F}(\mathbf{S}(\mathbf{X}, t)) \geq 0\}$. The phase-field regularization is detailed in the End Matter Appendix B; a finite-element implementation of the model in the open-source platform FEniCS is available on GitHub [41].

We applied the strength-constrained phase-field model to the full experimental geometry of Knauss (Fig. 1(a)), without introducing stochastic material properties or a defect distribution around the crack. The initial crack surface is planar, with no imposed crack-front undulations. Remarkably, the model naturally predicts the formation of echelon cracks, as shown in Fig. 1(d). The cracks are inclined at an angle of approximately 40° to

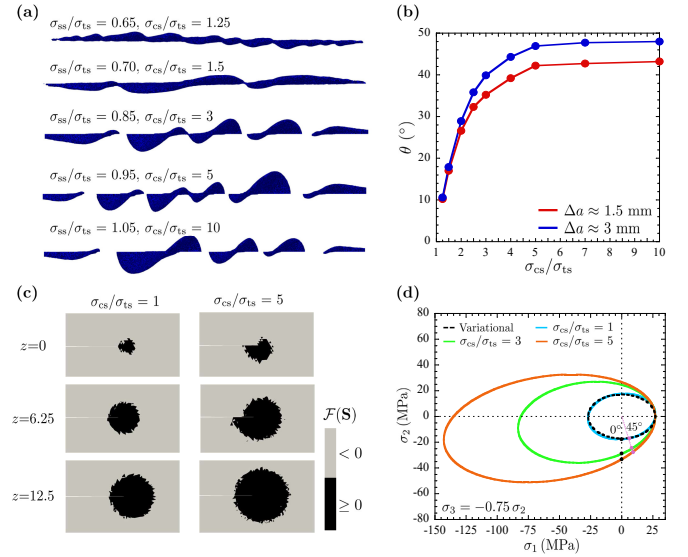


Figure 3. (a) Crack contours for five increasing values of the shear-to-tensile strength ratio, σ_{ss}/σ_{ts} , along with the corresponding compressive-to-tensile strength ratios, σ_{cs}/σ_{ts} . (b) Orientation angle for the largest daughter crack as a function of σ_{cs}/σ_{ts} for two values of crack extension Δa . (c) Contour plot around the crack front of the regions of the specimen where the stress field exceeds the strength surface ($\mathcal{F}(\mathbf{S}) = 0$) at three different locations (coordinate in mm) along the thickness and applied displacement $u = 0.075$ mm. (d) A 2D cut of the strength surface plotted in terms of the principal stresses σ_1 and σ_2 corresponding to the $\sigma_3 = -0.75 \sigma_2$ plane.

the original crack axis, which is close to the experimentally reported value. Importantly, this is the same phase-field model previously validated across a wide range of problems, such as indentation, torsion, and pokerchip tests, without any problem-specific modifications. The material parameters in equations (9)—elasticity, toughness, and strength—are standard, experimentally measurable quantities. Unlike prior analyses, the strength-constrained model predicts echelon crack growth without ad hoc assumptions.

For further study, we again adopt the smaller geometry (Fig. 2(a)) and simulate the problem for graphite and PDMS, capturing the fragmentation and evolution of the initial crack front. See End Matter Appendix C for a discussion of the formation and growth of echelon cracks; see also Supplemental Material, movies S1–S4 [31].

The question then arises: why does the strength-constrained phase-field model succeed where the classical variational model fails? To address this, we examine the influence of a key non-dimensional parameter—the ratio of shear to tensile strength, σ_{ss}/σ_{ts} , which directly enters the model. For graphite, we vary this ratio from 0.65 to 1.05. In terms of the corresponding ratio of compressive to tensile strength, $\sigma_{cs}/\sigma_{ts} = \sqrt{3} \sigma_{ss} \sigma_{ts} / (2 \sigma_{ts} - \sqrt{3} \sigma_{ss})$, this spans 1.25 to 10. Crack contours for a maximum ex-

tension of $\Delta a = 3$ mm are shown in Fig. 3(a).

We observe that for large strength ratios, echelon crack growth occurs, whereas for small ratios the phase-field crack front remains connected and undulating, with the amplitude of the undulations diminishing as σ_{ss}/σ_{ts} approaches 0.65, ultimately yielding an almost planar front. The orientation angle of the largest crack, θ , was computed for two crack extensions, $\Delta a = 1.5$ mm and 3 mm, in each case and plotted in Fig. 3(b). The angle transitions from approximately 45° for large σ_{ss}/σ_{ts} (or σ_{cs}/σ_{ts}) to near 0° for small values. The angle evolves as the crack gets longer. Since most brittle materials have $\sigma_{cs}/\sigma_{ts} > 3$, an angle of roughly 45° for large ratios aligns with experimental observations and the largest tensile stress orientation under pure mode III, whereas maximum energy release rate criteria predict planar growth ($\theta = 0^\circ$).

This analysis demonstrates that the strength-constrained model interpolates naturally between energy-based and stress-based predictions depending on the shear-to-tensile strength ratio. Consequently, the different empirical stress and energy-based criteria proposed in the literature can be reconciled within this unified framework.

To further understand why crack orientation depends on σ_{ss}/σ_{ts} or σ_{cs}/σ_{ts} , we plot a two-dimensional cut of the strength surface in terms of the principal stresses σ_1 and σ_2 for different values of σ_{cs}/σ_{ts} in Fig. 3(d). For comparison, we also include a strength surface inferred from the classical variational model, even though it is not explicitly included in that formulation. The 2D cut is taken along the plane $\sigma_3 = -0.75\sigma_2$, which approximates the relationship between the maximum and minimum principal stresses ahead of the crack in this tearing problem. For $\sigma_{cs}/\sigma_{ts} = 1$, the strength surface closely matches the inferred surface from the variational model, explaining why both models predict similar crack growth under this condition.

We also examine the directions of stress evolution in front of cracks oriented at 0° and 45° . The analysis shows that violations of the strength surface occur more readily at 45° for larger σ_{cs}/σ_{ts} . As noted in a recent work [40], the growth of a large crack occurs only in regions where the strength criterion is exceeded. Hence, when shear strength is high, the material preferentially fails under tension, causing the parent crack to curve out of the plane and often fragment into daughter cracks. Figure 3(c) shows the regions near the crack front where the strength surface is exceeded for an applied displacement of $u = 0.075$ mm. As one moves away from the mid-plane of the domain ($z = 12.5$ mm), the strength violation becomes increasingly asymmetric for larger values of σ_{cs}/σ_{ts} . Conversely, when shear strength is low, the crack favors planar propagation under shear since the strength violation is symmetric around the crack front across the thickness (Fig. 3(c)). While this behav-

ior is intuitive, crack formation is also influenced by the material's fracture toughness. In regions exceeding the strength surface, the strength-constrained model drives crack growth by minimizing the combined elastic and surface energies [40]. Therefore, the precise pattern of crack formation cannot be predicted by strength considerations alone.

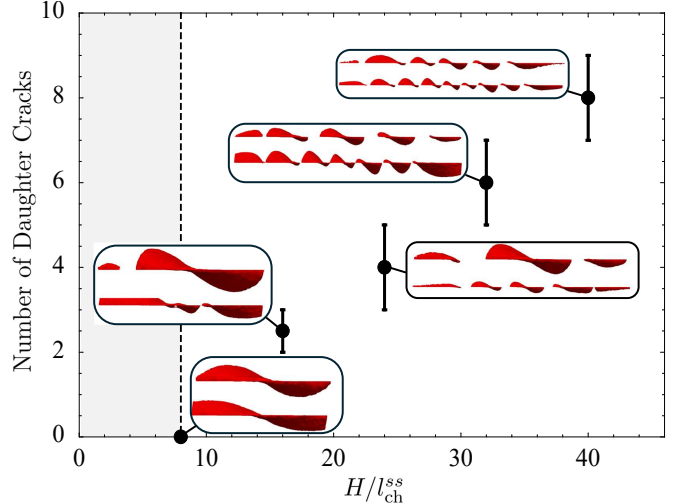


Figure 4. Number of daughter cracks as a function of H/l_{ch}^{ss} . Inset panels (top) show results obtained by varying l_{ch}^{ss} via changes in G_c , E , or σ_{ss} ; inset panels (bottom) show results obtained by varying H . Error bars indicate the range of observed crack counts. No echelon cracks observed in the gray shaded region.

We further investigated the influence of material toughness and, more generally, the fracture process zone size on echelon crack formation. The fracture process zone is associated with a characteristic length scale emerging from the governing equations (9). Specifically, the elastic energy density $W(\mathbf{F})$ and the strength surface $\mathcal{F}(\mathbf{S}) = 0$ have units of force per unit area, while the toughness G_c has units of force per unit length. Their combination defines a family of intrinsic material length scales. For the present problem, where the stress state is predominantly shear, we consider the linear-elastic shear-based length scale

$$l_{ch}^{ss} = \frac{3G_c E}{8\sigma_{ss}^2}, \quad (6)$$

where E is the Young's modulus. We performed three sets of simulations, individually varying G_c , E , and σ_{ss}^2 by factors of 1–5 from their default values while keeping all other material and geometric parameters fixed. For each case, we recorded the number of daughter cracks that formed. The regularization length ε was maintained at $\varepsilon/l_{ch}^{ss} = 1/3$. We observe that the initial number of cracks increases as this ratio decreases, although it converges for sufficiently small values. Once cracks have grown to approximately 10ε , the number of daughter

cracks is largely insensitive to $\varepsilon/l_{\text{ch}}^{\text{ss}}$, as smaller cracks either coalesce rapidly or stop growing due to shielding effects.

Remarkably, both the number and orientation of daughter cracks were found to depend primarily on the value of $l_{\text{ch}}^{\text{ss}}$, regardless of whether G_c , E , or σ_{ss} was varied. The results, shown in Fig. 4 (top row of each inset panel), indicate that the number of daughter cracks decreases as $l_{\text{ch}}^{\text{ss}}$ increases. For sufficiently large $l_{\text{ch}}^{\text{ss}}$, echelon cracks no longer form, and the crack evolves as a continuous, curved front. These observations are consistent with Ronsin et al. [4], who reported that dissipative gels under a lower energy release rate, associated with a smaller process zone [42], exhibit echelon cracking, whereas under a higher energy release rate, favor smooth, curved cracks.

We also performed simulations keeping $l_{\text{ch}}^{\text{ss}}$ constant while varying the plate width H (Fig. 2(a)) by a factor of 1–5, maintaining $\varepsilon/l_{\text{ch}}^{\text{ss}}$ fixed. The results, shown in Fig. 4 (bottom row of each inset panel), reveal that reducing H by a factor of 5 has a similar effect as increasing $l_{\text{ch}}^{\text{ss}}$ fivefold. This suggests that echelon crack formation is governed by the non-dimensional parameter $H/l_{\text{ch}}^{\text{ss}}$.

To summarize, we have shown through an example that Griffith's theory, when cast into the variational phase-field model, is incomplete for predicting the growth of a large crack. The underlying reason is that the energetic Griffith theory does not account for the restrictions imposed by the strength surface on crack evolution. A phase field model that performs a strength-constrained minimization can naturally reproduce echelon crack nucleation and evolution without defects, stochasticity, or ad hoc assumptions, although further validation with more experiments should be conducted. Crack orientation and fragmentation are controlled by two key non-dimensional parameters: the shear-to-tensile strength ratio, $\sigma_{\text{ss}}/\sigma_{\text{ts}}$, and the plate-thickness-to-characteristic-length ratio, $H/l_{\text{ch}}^{\text{ss}}$.

Combined with validation studies performed in previous works, these results demonstrate that the strength-constrained phase-field framework [28, 33] can robustly predict arbitrary fracture initiation and propagation in soft and hard isotropic brittle materials. This approach is also easily extendable to anisotropic materials. Thus, it may provide a resolution to the century-old question of when and where cracks grow.

Acknowledgments— The authors would like to acknowledge the financial support from the National Science Foundation, United States, through the grant CMMI-2404808.

-
- [1] A. A. Griffith, VI. the phenomena of rupture and flow in solids, *Philosophical transactions of the royal society of london. Series A, containing papers of a mathematical or physical character* **221**, 163 (1921).
 - [2] E. Sommer, Formation of fracture 'lances' in glass, *Engineering Fracture Mechanics* **1**, 539 (1969).
 - [3] W. Knauss, An observation of crack propagation in anti-plane shear, *International Journal of Fracture Mechanics* **6**, 183 (1970).
 - [4] O. Ronsin, C. Caroli, and T. Baumberger, Crack front echelon instability in mixed mode fracture of a strongly nonlinear elastic solid, *Europhysics Letters* **105**, 34001 (2014).
 - [5] K. Pham and K. Ravi-Chandar, On the growth of cracks under mixed-mode I+III loading, *International Journal of Fracture* **199**, 105 (2016).
 - [6] M. Wang, M. Adda-Bedia, J. M. Kolinski, and J. Fineberg, How hidden 3D structure within crack fronts reveals energy balance, *Journal of the Mechanics and Physics of Solids* **161**, 104795 (2022).
 - [7] M. L. Cooke and D. D. Pollard, Fracture propagation paths under mixed mode loading within rectangular blocks of polymethyl methacrylate, *Journal of Geophysical Research: Solid Earth* **101**, 3387 (1996).
 - [8] E. A. Zimmermann, M. E. Launey, H. D. Barth, and R. O. Ritchie, Mixed-mode fracture of human cortical bone, *Biomaterials* **30**, 5877 (2009).
 - [9] A. T. Zehnder and N. K. Zella, Spiral to flat fracture transition for notched rods under torsional loading, *International Journal of Fracture* **195**, 87 (2015).
 - [10] G. Barenblatt and G. Cherepanov, On brittle cracks under longitudinal shear, *Journal of Applied Mathematics and Mechanics* **25**, 1654 (1961).
 - [11] F. Erdogan and G. Sih, On the crack extension in plates under plane loading and transverse shear, *Journal of basic engineering* **85**, 519 (1963).
 - [12] G. C. Sih, Strain-energy-density factor applied to mixed mode crack problems, *International Journal of Fracture* **10**, 305 (1974).
 - [13] R. V. Gol'dstein and R. L. Salganik, Brittle fracture of solids with arbitrary cracks, *International Journal of Fracture* **10**, 507 (1974).
 - [14] R. Nuismer, An energy release rate criterion for mixed mode fracture, *International Journal of Fracture* **11**, 245 (1975).
 - [15] C.-H. Wu, Fracture under combined loads by maximum-energy-release-rate criterion, *Journal of Applied Mechanics* **45**, 553 (1978).
 - [16] V. Lazarus, F.-G. Buchholz, M. Fulland, and J. Wiebelsiek, Comparison of predictions by mode II or mode III criteria on crack front twisting in three or four point bending experiments, *International Journal of Fracture* **153**, 141 (2008).
 - [17] A. Chambolle, G. A. Francfort, and J.-J. Marigo, When and how do cracks propagate?, *Journal of the Mechanics and Physics of Solids* **57**, 1614 (2009).
 - [18] K. Pham and K. Ravi-Chandar, The formation and growth of echelon cracks in brittle materials, *International Journal of Fracture* **206**, 229 (2017).
 - [19] B. Mittelman and Z. Yosibash, Energy release rate cannot predict crack initiation orientation in domains with a

- sharp V-notch under mode III loading, *Engineering Fracture Mechanics* **141**, 230 (2015).
- [20] A. J. Pons and A. Karma, Helical crack-front instability in mixed-mode fracture, *Nature* **464**, 85 (2010).
- [21] J.-B. Leblond, A. Karma, and V. Lazarus, Theoretical analysis of crack front instability in mode I+ III, *Journal of the Mechanics and Physics of Solids* **59**, 1872 (2011).
- [22] I. Kolvin, G. Cohen, and J. Fineberg, Topological defects govern crack front motion and facet formation on broken surfaces, *Nature materials* **17**, 140 (2018).
- [23] G. A. Francfort and J.-J. Marigo, Revisiting brittle fracture as an energy minimization problem, *Journal of the Mechanics and Physics of Solids* **46**, 1319 (1998).
- [24] A. Chambolle, G. A. Francfort, and J.-J. Marigo, Revisiting energy release rates in brittle fracture, *Journal of Nonlinear Science* **20**, 395 (2010).
- [25] G. Francfort, Variational fracture: twenty years after, *International Journal of Fracture* **237**, 3 (2022).
- [26] B. Bourdin, G. A. Francfort, and J.-J. Marigo, Numerical experiments in revisited brittle fracture, *Journal of the Mechanics and Physics of Solids* **48**, 797 (2000).
- [27] S. Sato, H. Awaji, K. Kawamata, A. Kurumada, and T. Oku, Fracture criteria of reactor graphite under multiaxial stresses, *Nuclear Engineering and Design* **103**, 291 (1987).
- [28] A. Kumar, B. Bourdin, G. A. Francfort, and O. Lopez-Pamies, Revisiting nucleation in the phase-field approach to brittle fracture, *Journal of the Mechanics and Physics of Solids* **142**, 104027 (2020).
- [29] X. Poulaïn, V. Lefevre, O. Lopez-Pamies, and K. Ravi-Chandar, Damage in elastomers: nucleation and growth of cavities, micro-cracks, and macro-cracks, *International Journal of Fracture* **205**, 1 (2017).
- [30] F. Kamarei, A. Kumar, and O. Lopez-Pamies, The poker-chip experiments of synthetic elastomers explained, *Journal of the Mechanics and Physics of Solids* **188**, 105683 (2024).
- [31] See Supplemental Material for additional methods and data.
- [32] G. Molnár, A. Doitrand, and V. Lazarus, Phase-field simulation and coupled criterion link echelon cracks to internal length in antiplane shear, *Journal of the Mechanics and Physics of Solids* **188**, 105675 (2024).
- [33] A. Kumar, G. A. Francfort, and O. Lopez-Pamies, Fracture and healing of elastomers: A phase-transition theory and numerical implementation, *Journal of the Mechanics and Physics of Solids* **112**, 523 (2018).
- [34] A. Kumar and O. Lopez-Pamies, The poker-chip experiments of Gent and Lindley (1959) explained, *Journal of the Mechanics and Physics of Solids* **150**, 104359 (2021).
- [35] A. Kumar, K. Ravi-Chandar, and O. Lopez-Pamies, The revisited phase-field approach to brittle fracture: application to indentation and notch problems, *International Journal of Fracture* **237**, 83 (2022).
- [36] A. Kumar, Y. Liu, J. E. Dolbow, and O. Lopez-Pamies, The strength of the brazilian fracture test, *Journal of the Mechanics and Physics of Solids* **182**, 105473 (2024).
- [37] C. Liu and A. Kumar, Emergence of tension-compression asymmetry from a complete phase-field approach to brittle fracture, *International Journal of Solids and Structures* **309**, 113170 (2025).
- [38] F. Kamarei, B. Zeng, J. E. Dolbow, and O. Lopez-Pamies, Nine circles of elastic brittle fracture: A series of challenge problems to assess fracture models, *Computer Methods in Applied Mechanics and Engineering* **448**, 118449 (2026).
- [39] U. Khayaz, A. Dahal, and A. Kumar, A comparison of phase field models of brittle fracture incorporating strength, I: Mixed-mode loading, *Engineering Fracture Mechanics* **330**, 111679 (2025).
- [40] O. Lopez-Pamies and F. Kamarei, When and where do large cracks grow? Griffith energy competition constrained by material strength, *Extreme Mechanics Letters* **81**, 102417 (2025).
- [41] O. Ward and A. Kumar, Data for echelon crack formation, <https://github.com/Aditya-Kumar-Lab-GT/Echelon-Crack-Formation> (2026), version 1.0.
- [42] J. Slootman, V. Waltz, C. J. Yeh, C. Baumann, R. Göstl, J. Comtet, and C. Creton, Quantifying rate-and temperature-dependent molecular damage in elastomer fracture, *Physical Review X* **10**, 041045 (2020).
- [43] F. Vicentini, C. Zolesi, P. Carrara, C. Maurini, and L. De Lorenzis, On the energy decomposition in variational phase-field models for brittle fracture under multiaxial stress states, *International Journal of Fracture* **247**, 291 (2024).
- [44] A. Santarossa, N. R. Varela-Rosales, P. Steinmann, and M. A. Moreno-Mateos, Configurational forces explain echelon cracks in soft materials, arXiv preprint arXiv:2507.12247 (2025).

END MATTER

Appendix A—In the literature [18, 32], it has been argued that the energy functional in the variational formulation needs to be modified via a strain-energy decomposition

$$\begin{aligned} \hat{\mathcal{E}}^{\varepsilon}(\mathbf{y}, z) = & \int_{\Omega_0} [z^2 W^+(\mathbf{F}) + W^-(\mathbf{F})] d\mathbf{X} \\ & + \frac{3G_c}{8} \int_{\Omega_0} \left(\frac{1-z}{\varepsilon} + \varepsilon \nabla z \cdot \nabla z \right) d\mathbf{X}, \end{aligned} \quad (7)$$

where W^+ denotes the tensile part of the strain energy degraded by the phase field and W^- the compressive part that does not drive fracture. The motivation for

this split is that the standard regularized formulation does not distinguish between crack faces under tension and compression: in the sharp crack setting, compressive loading enforces contact and allows force transmission, whereas in the regularized model, all energy is degraded, preventing such transfer. This leads to violations of material impenetrability and permits crack growth under compression, contrary to experimental observations. Although the split formulation has been proposed as a remedy, there is no rigorous and general procedure for decomposing an arbitrary strain-energy density into tensile and compressive parts in two or three dimensions [39].

In particular, the spectral split (7) introduces unphysical residual shear stresses along cracks [37, 43], rendering it unphysical for shear-dominated fracture.

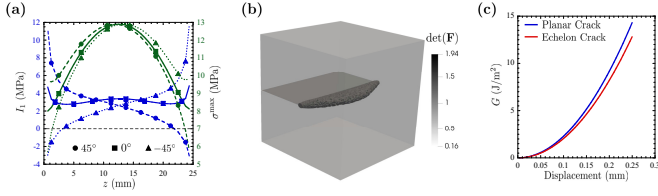


Figure 5. (a) First invariant of the stress tensor (left axis) and maximum principal stress (right axis) plotted as a function of z coordinate in front of the crack. (b) Plot of the determinant of the deformation gradient tensor over the propagating crack. (c) Plot of the energy release rate for a planar and echelon crack growth.

Furthermore, our analysis shows that an energy split should not be needed for the present problem. As shown in Fig. 5(b), even in the large-deformation regime, the determinant of the deformation gradient remains well above zero, indicating that material interpenetration does not occur and crack faces are not in contact; for small deformations, $\det(\mathbf{F})$ remains close to unity. Stress analysis further supports this conclusion. For planar crack growth (corresponding to the 0° orientation in Fig. 2(a)), the first stress invariant I_1 is strictly positive ahead of the crack across the thickness (Fig. 5(a)), indicating a substantial opening mode; the normal stress component S_{yy} is also positive. As an additional check, we computed the energy release rate, G , for both planar and echelon cracks using

$$G \approx -\frac{\mathcal{W}(u, A + \Delta A) - \mathcal{W}(u, A)}{\Delta A}, \quad (8)$$

where $\mathcal{W} = \int_{\Omega_0} W(\mathbf{F}) d\mathbf{X}$ is the total strain energy, A is the initial crack surface area, and $\Delta A = A/50$ is the area increment. The results, shown in Fig. 5(c), demonstrate that the planar crack has a higher energy release rate and is therefore energetically favored, consistent with the phase-field predictions. Therefore, the variational formulation, contrary to prior claims in the literature, predicts a crack path that is experimentally inconsistent.

Appendix B— The strength surface (4) constraint is applied to the variational phase-field model (3) through a two-step procedure: (i) consider the Euler-Lagrange equations of the variational principle (3) as the primal model, and (ii) introduce the strength surface by adding a stress-based driving force to the Euler-Lagrange equation for the phase-field evolution. The resulting formulation says that, subject to the appropriate initial and boundary conditions, the deformation field \mathbf{y} and the phase field z are obtained from solving two partial differential

equations

$$\begin{cases} \text{Div} \left(z^2 \frac{\partial W}{\partial \mathbf{F}} (\nabla \mathbf{y}) \right) = 0, \\ \frac{3}{4} \text{Div} [\varepsilon \delta^\varepsilon G_c \nabla z] = 2z W(\nabla \mathbf{y}) + c_e - \frac{3}{8} \frac{\delta^\varepsilon G_c}{\varepsilon}, \end{cases} \quad (9)$$

subject to $z < 0$, where the term $c_e(\mathbf{X}, t)$ is the additional driving force and δ^ε is a non-negative coefficient, both of whose prescriptions depend on the particular form of strength surface. As explained in a recent work [40], these equations describe a constrained minimization problem: crack growth happens in regions where the strength surface has been met through a minimization of the sum of elastic and surface energies.

The formulation allows for an arbitrary choice of the strength surface. In this work, we have adopted the Drucker-Prager (DP) surface, expressed as follows:

$$\mathcal{F}(\mathbf{S}) = \sqrt{J_2} + \gamma_1 I_1 + \gamma_0 = 0, \quad (10)$$

with

$$\gamma_0 = -\sigma_{ss}, \quad \gamma_1 = \frac{\sqrt{3}\sigma_{ss} - \sigma_{ts}}{\sqrt{3}\sigma_{ts}}, \quad (11)$$

where

$$I_1 = \text{tr } \mathbf{S}, \quad J_2 = \frac{1}{2} \text{tr } \mathbf{S}_D^2, \quad \mathbf{S}_D = \mathbf{S} - \frac{1}{3}(\text{tr } \mathbf{S})\mathbf{I}, \quad (12)$$

stand for two of the standard invariants of the stress tensor \mathbf{S} , while the constants $\sigma_{ts} > 0$ and $\sigma_{ss} > 0$ denote the uniaxial tensile and shear strengths of the material, respectively. Corresponding to the DP surface, the functional form for $c_e(\mathbf{X}, t)$ was presented recently in [30]:

$$c_e(\mathbf{X}, t) = \beta_2^\varepsilon z^2 \sqrt{J_2} + \beta_1^\varepsilon z^2 I_1 - z \left(1 - \frac{|I_1|}{I_1} \right) W(\mathbf{F}). \quad (13)$$

where β_1^ε and β_2^ε are ε -dependent coefficients

$$\begin{cases} \beta_1^\varepsilon = \frac{1}{\sigma_{hs}} \delta^\varepsilon \frac{G_c}{8\varepsilon} - \frac{2W_{hs}}{3\sigma_{hs}} \\ \beta_2^\varepsilon = \frac{\sqrt{3}(3\sigma_{hs} - \sigma_{ts})}{\sigma_{hs}\sigma_{ts}} \delta^\varepsilon \frac{G_c}{8\varepsilon} + \frac{2W_{hs}}{\sqrt{3}\sigma_{hs}} - \frac{2\sqrt{3}W_{ts}}{\sigma_{ts}} \end{cases}. \quad (14)$$

Here, where W_{ts} and W_{hs} stand for the values of the stored-energy function along uniform uniaxial tension and hydrostatic stress states at which the strength surface is violated. σ_{hs} is the hydrostatic strength which for the DP surface is obtained as $\sigma_{hs} = \sigma_{ss}\sigma_{ts}/(3\sigma_{ss} - \sqrt{3}\sigma_{ts})$. The coefficient δ^ε is obtained as

$$\begin{aligned} \delta^\varepsilon = & \left(1 + \frac{3}{8} \frac{h}{\varepsilon} \right)^{-2} \left(\frac{\sigma_{ts} + (1 + 2\sqrt{3})\sigma_{hs}}{(8 + 3\sqrt{3})\sigma_{hs}} \right) \frac{3G_c}{16W_{ts}\varepsilon} \\ & + \left(1 + \frac{3}{8} \frac{h}{\varepsilon} \right)^{-1} \frac{2}{5}, \end{aligned} \quad (15)$$

where h denotes the finite element size.

Appendix C— The results with the strength-constrained phase field for the smaller geometry (Fig. 2(a)) with Graphite and PDMS are shown in Fig. 6. Crack contours are shown at $z = 0.1$ for three applied displacements in each case. See Supplemental Material movies S1-S4 for the full evolution of cracks. In graphite, four daughter cracks initially form near the center, disconnected from one another but connected to the parent crack, then reorient and propagate toward the lateral boundaries, with additional daughter cracks forming near the edges. As growth continues, the cracks eventually begin to bridge. In the nearly incompressible PDMS, daughter cracks first appear near the lateral surfaces and later in the center of the domain. They are inclined at a larger angle compared to those observed for Graphite. This is because the ratio of compressive strength to tensile strength for PDMS is double that of Graphite. As shown in Fig. 3(b), the orientation angle increases with this ratio. Detailed analysis of crack spacing, reorientation, and coalescence is beyond the scope of this work;

extensive studies addressing these phenomena for hard brittle materials are available in the literature [18, 44].

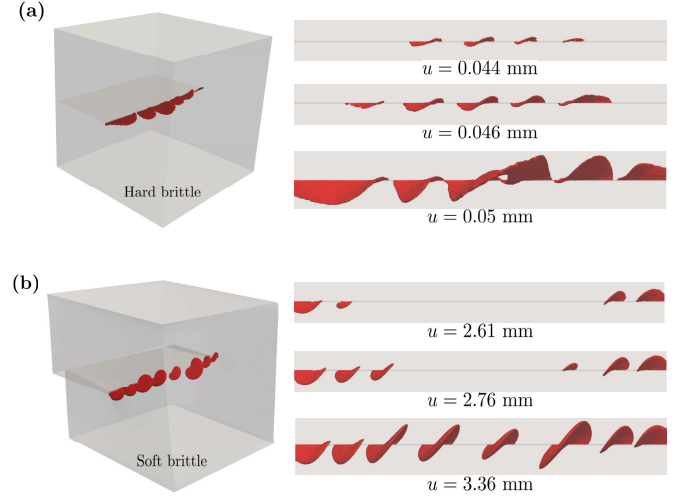


Figure 6. Simulations with the strength-constrained phase field model. Crack path contour for three values of applied displacement, u , for (a) Graphite, and (b) PDMS.